REPORT DOCUMENTATION PAGE

Form Approved
OMB No. 0704-0188

1. REPORT DATE *(DD-MM-YYYY)*	**2. REPORT TYPE**	**3. DATES COVERED** *(From - To)*
01-08-2006	JOURNAL ARTICLE	1 Oct 2004 – 1 Dec 2005

4. TITLE AND SUBTITLE

Micromachined Rectangular-Coaxial Transmission Lines

5a. CONTRACT NUMBER

5b. GRANT NUMBER

5c. PROGRAM ELEMENT NUMBER
61102F

6. AUTHOR(S)

J. Robert Reid, Eric D. Marsh and Richard T. Webster

5d. PROJECT NUMBER
2305

5e. TASK NUMBER
HA

5f. WORK UNIT NUMBER
01

7. PERFORMING ORGANIZATION NAME(S) AND ADDRESS(ES)
Antenna Technology Branch (AFRL/SNHA)
80 Scott Dr.
Hanscom AFB, MA 01731

8. PERFORMING ORGANIZATION REPORT

9. SPONSORING / MONITORING AGENCY NAME(S) AND ADDRESS(ES)
Electromagnetics Technology Division
Sensors Directorate
Air Force Research Laboratory
80 Scott Drive
Hanscom AFB MA 01731-2909

10. SPONSOR/MONITOR'S ACRONYM(S)
AFRL-SN-HS

11. SPONSOR/MONITOR'S REPORT NUMBER(S)
AFRL-SN-HS-JA-2006-0062

12. DISTRIBUTION / AVAILABILITY STATEMENT
DISTRIBUTION STATEMENT A. Approved for public release; distribution is unlimited.

13. SUPPLEMENTARY NOTES
Clearance Number ESC-06-0062

14. ABSTRACT
Rectangular-coaxial (recta-coax) transmission lines fabricated through a three-dimensional micromachining process are presented. These lines are shown to have significant advantages over competing integrated transmission lines such as microstrip and coplanar waveguides. Design equations are presented for impedance, loss, and frequency range. The equations are confirmed with simulations and measurements. The quality factor of shorted lambda/4 resonators is measured to be 156 at 60 GHz. This corresponds to a line loss of 0.353 dB/cm. Advantages of these lines for passive millimeter-wave circuits including ease of signal routing, high isolation, and signal crossovers are demonstrated with realized lines and couplers.

15. SUBJECT TERMS
Coplanar waveguides, couplers, filters, microstrip, millimeter-wave circuits, resonators

16. SECURITY CLASSIFICATION OF:			**17.LIMITATION OF ABSTRACT**	**18.NUMBER OF PAGES**	**19a. NAME OF RESPONSIBLE PERSON**
a. REPORT	**b. ABSTRACT**	**c.THIS PAGE**	Unlimited	10	J. Robert Reid
Unclassified	Unclassified	Unclassified			**19b. TELEPHONE NUMBER** *(include area code)* N/A

Standard Form 298 (Rev. 8-98)
Prescribed by ANSI Std. Z39.18

Micromachined Rectangular-Coaxial Transmission Lines

J. Robert Reid, *Member, IEEE*, Eric D. Marsh, *Member, IEEE*, and Richard T. Webster, *Senior Member, IEEE*

***Abstract*—Rectangular-coaxial (recta-coax) transmission lines fabricated through a three-dimensional micromachining process are presented. These lines are shown to have significant advantages over competing integrated transmission lines such as microstrip and coplanar waveguides. Design equations are presented for impedance, loss, and frequency range. The equations are confirmed with simulations and measurements. The quality factor of shorted $\lambda/4$ resonators is measured to be 156 at 60 GHz. This corresponds to a line loss of 0.353 dB/cm. Advantages of these lines for passive millimeter-wave circuits including ease of signal routing, high isolation, and signal crossovers are demonstrated with realized lines and couplers.**

***Index Terms*—Coplanar waveguides (CPWs), couplers, filters, microstrip, millimeter-wave circuits, resonators.**

I. Introduction

INCREASING use of the microwave spectrum combined with the demand for high bandwidth secure communications is increasingly pushing users towards millimeter-wave frequencies. However, the design of circuits above 30 GHz is complicated by signal crosstalk and the tight fabrication tolerances required to ensure accurate reproduction of simulated circuit designs. Over the past several years, the development of multilayer electroplated metal micromachining processes has made it possible to realize integrated rectangular-coaxial (recta-coax) transmission lines such as that illustrated in Fig. 1. These lines have the potential to greatly simplify the design of passive millimeter-wave circuits.

Recta-coax lines consist of a rectangular center line suspended in air and enclosed on all sides by a ground plane. They are similar to microstrip and coplanar waveguide (CPW) lines in that they are fabricated using thin-film processing on top of a flat substrate. It is, therefore, possible to route the lines along any two-dimensional path. Further, the lines can be integrated on top of substrates such as silicon, gallium arsenide, and alumina. However, recta-coax lines offer significant advantages over both CPW and microstrip transmission lines. First, they are TEM and not quasi-TEM, mitigating dispersion, thus allowing operation over a very broad frequency range (dc to over 200 GHz). Second, the fields are completely enclosed by the ground. Therefore, two lines can be routed very close to each other. More importantly, the lines can easily cross paths without significant signal interference. Third, the design and performance of the lines are independent of the substrate. This eliminates the need for substrate thinning, and allows the substrate to be chosen based on parameters such as cost and the requirements of active devices. It also allows designs to be implemented on multiple substrates without any changes.

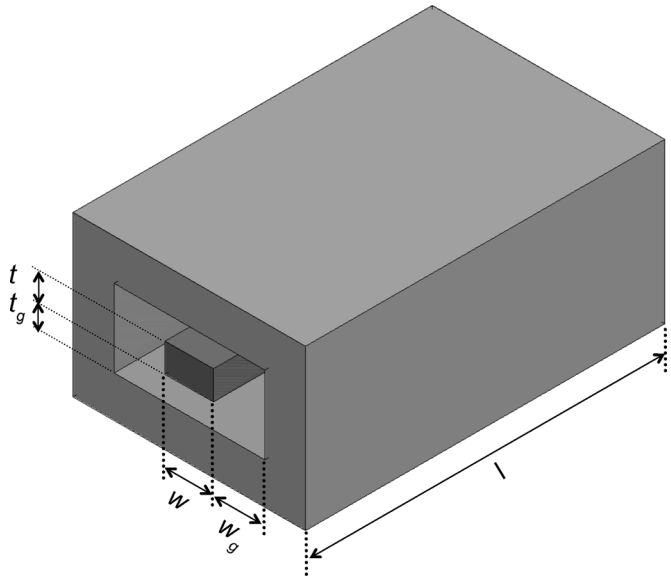

Fig. 1. Schematic illustration of a recta-coax line labeling the design dimensions.

The earliest investigations of micromachined transmission lines utilized bulk etching of silicon to form lines on thin membranes [1], [2]. In that study, the lines were referred to as microshield lines. The lines were implemented as coplanar transmission lines on a thin membrane with an air-filled metal cavity under the lines. In some cases, a second metal cavity was added above the line as well to create an entirely enclosed structure. The design of the CPW had to be modified to account for the additional capacitive loading of the added cavity ground planes. In addition, removing nearly all of the dielectric allowed the lines to operate in an effectively pure TEM mode [2]. The lines were fabricated by bulk etching of the back side of multiple silicon wafers. Metalizations were then added, and two or three wafers were bonded together. In subsequent studies, the microshield lines were designed to take on more of a microstrip style and then used in a large variety of millimeter-wave circuit demonstrations [3]–[9]. Of particular note is the exceptional millimeter-wave filter performance achieved [5]–[7]. Unfortunately, the complexity of the fabrication has limited the

Manuscript received December 15, 2005; revised April 2, 2006. This work was supported in part by the Air Force Office of Scientific Research under LRIR 92SN04COR and in part by the Center for Advanced Sensor and Communications Antennas.

The authors are with the Antenna Technology Branch, Air Force Research Laboratory, Hanscom AFB, MA 01731 USA (e-mail: James.Reid@hanscom.af.mil).

Digital Object Identifier 10.1109/TMTT.2006.879133

commercial acceptance of the microshield lines. One attempt to address this is the work of Melanović *et al.* [10], [11], in which CPWs were also formed on membranes. However, the lines were formed using post processing of CMOS wafers. The final bulk etch was done after all of the lines were patterned. That approach does not provide a cavity around the CPW, but does eliminate dielectric losses. Neither of these approaches allows the flexibility and complex routing provided by the recta-coax lines described in this paper.

Approaches utilizing SU-8 and polymer films to create microstrip on a thin film [12], CPW on thin film [13], and membrane-supported CPW lines [14], [15] have also been demonstrated. These polymer approaches typically offer simpler fabrication, but for microstrip lines offer high losses. Very low losses (0.18 dB/cm at 20 GHz) have been reported for large CPW lines on SU-8 films by etching out the SU-8 in the gap region between the lines. However, this technique is not suitable for multiple layers of transmission lines. In the case of membrane-supported CPW lines, relatively low losses (0.7 dB/cm) have been reported at W-band when the line is fully enclosed [14]; however, the enclosure process is not detailed and is not inherent to the line as fabricated, and the design of multiple conductor layers would be difficult for the process as described.

Over the past several years, work has progressed on the fabrication of transmission lines using electroplated films on top of the substrate, leading to the realization of suspended CPW transmission lines [16]–[20] and recta-coax lines [18]–[26]. Demonstrations of couplers and filters at microwave frequencies have shown the potential for these lines to simplify the design of millimeter-wave systems [21], [23]–[26]. This paper provides a detailed description of integrated recta-coax lines including design equations for impedance, loss, and resonator quality factor. Calculations from these equations are compared with Ansoft's High Frequency Structure Simulator (HFSS) [27] simulations and measured values. In addition, examples of the transmission lines are provided, including lines of different lengths, lines with bends, and 60-GHz couplers.

II. Recta-Coax Design Equations

A. Characteristic Impedance

The characteristic impedance of a transmission line can be calculated as

$$Z_0 = \sqrt{\frac{L_{\rm len}}{C_{\rm len}}} = \frac{1}{\nu_p C_{\rm len}} \tag{1}$$

where $\nu_p = 2.998 \cdot 10^8$ (m/s) is the phase velocity of the line, which is equal to the speed of light in vacuum for an air core TEM transmission line, and $C_{\rm len}$ is the capacitance per unit length of the transmission line. It is, therefore, only necessary to solve for the capacitance per unit length between the center line and the ground. Chen [28] provides equations for solving this capacitance over a range of possible line dimensions. For lines where the width and thickness are larger than the gaps ($w > w_g$ and $t > t_g$), the capacitance is calculated as

$$\begin{aligned} C_{\rm len} = {} & 2\epsilon\left(\frac{w}{t_g} + \frac{t}{w_g}\right) \\ & + \frac{4\epsilon}{\pi}\left[ln\left(\frac{w_g^2 + t_g^2}{4t_g^2}\right) + 2\frac{t_g}{w_g}\arctan\left(\frac{w_g}{t_g}\right)\right] \\ & + \frac{4\epsilon}{\pi}\left[ln\left(\frac{w_g^2 + t_g^2}{4w_g^2}\right) + 2\frac{w_g}{t_g}\arctan\left(\frac{t_g}{w_g}\right)\right] \end{aligned} \tag{2}$$

where all dimensions are defined in Fig. 1 and $\epsilon = \epsilon_0 = 8.85$ pF/m is the permittivity of the dielectric. Without loss of generality, it is assumed that $w \geq t$. For lines that are thin, i.e., $t < t_g$, the corner capacitances cannot be considered independently and the capacitance is calculated as

$$\begin{aligned} C_{\rm len} = {} & 2\frac{\epsilon w}{t_g} + \frac{4\epsilon}{\pi ln(2)}\left[1 + \coth\left(\frac{\pi w_g}{2t_g + t}\right)\right] \\ & \cdot \left[\frac{t + 2t_g}{2t_g} ln\left(\frac{4t_g + t}{t}\right) + ln\left(\frac{t(4t_g + t)}{4t_g^2}\right)\right]. \end{aligned} \tag{3}$$

Chen does not provide an estimate as to the accuracy of these equations. Weil provides a review of the methods for calculating this capacitance [29], and notes that Chen's work is based on the coupled stripline equations developed by Cohn [30], and these equations are only valid when $w > 0.35(w + 2w_g)$, which can be approximated by the condition $w > w_g$. In order to confirm the validity of Chen's equations and get an approximation of their accuracy for the types of lines that can be fabricated with integrated processes, calculations using (2) and (3) were compared with finite-element simulations performed using Ansoft's HFSS. The line dimensions used for this comparison are shown in Table I. Calculations and simulations were done by fixing t, t_g, and w_g, and then varying w over the range shown in the $w_{\rm range}$ column in Table I. When using the equations as defined above, the calculated value was within 4% of the simulation in all cases. While this is not a rigorous analysis, it does give us confidence that Chen's equations are accurate for the lines that can be realized. More exact methods of calculating this capacitance for these cases have been detailed by other authors, but are not considered here [31]–[37].

TABLE I
Possible Line Configurations for Integrated Recta-Coax

Line	t	t_g	w_g	w_{range}	C_{len} (pF/m)	Z_0 (Ω)
A	28	24	50	20-100	47.8-106.7	69.8-31.2
B	44	16	20	20-100	81.2-169.7	41.1-19.7
C	33	30	65	20-150	44.3-121.0	75.3-27.6
D	30	32	50	20-150	41.7-113.6	80.0-29.4
E	30	122	150	30-600	26.3-108.9	127.1-30.7

(All dimensions in μm)

B. Line Loss

The loss of a transmission line is evaluated as the sum of conductor and dielectric losses. For an air core TEM transmission line, it is reasonable to ignore the dielectric loss and calculate

only the conductor loss α_c. The conductor loss is calculated using the Wheeler incremental inductance rule as [38]

$$\alpha_c = \frac{P_{lc}}{2P_0} \tag{4}$$

where P_{lc} is the power loss in the conductor per unit length, and $P_0 = |V|^2/(2Z_0)$ is the reference power. The power loss can be calculated as

$$P_{lc} = |I|^2 R = \frac{|I|^2 \Delta L}{\sigma \mu_c \delta_s^2} \tag{5}$$

where R is the line resistance, ΔL is the change in inductance when all conductor walls are receded by an amount $\delta_s/2$, and σ, μ_c, and $\delta_s = \sqrt{2/\omega\mu_c\sigma}$ are the conductivity, permeability, and skin depth of the metal, respectively. Substituting values for P_{lc} and P_0 into (4) and simplifying results in

$$\alpha_c = \frac{\Delta L}{\sigma \mu_c \delta_s^2 Z_0}. \tag{6}$$

Since the inductance is related to the characteristic impedance as $Z_0 = L\nu_p$, the incremental inductance is related as $\Delta Z_0 = \Delta L \nu_p$, and (6) can be rewritten in terms of the change in the characteristic impedance to get

$$\alpha_c = \frac{\Delta Z_0}{\sigma \mu_c \nu_p \delta_s^2 Z_0} \tag{7}$$

where Z_0 is the impedance calculated as described in Section II-A, and ΔZ_0 is the change in the impedance when the conductor walls are receded by half the skin depth of the conductor $\delta_s/2$. This equation is not the same as that reported by Lau [39] because Lau uses the approximation $Z_0(\delta_s/2) \simeq Z_0 + (\delta_s/2)(\partial Z_0/\partial \ell)$. While this approximation is generally accurate for good conductors, it is not necessary given the widespread availability of digital computers to directly evaluate ΔZ_0. This has the added advantage that any method for calculating Z_0 including simulation can be used.

The conductor loss must also account for metal roughness. This is done by adding a correction factor as given by Edwards [40]

$$\alpha_c' = \alpha_c \left[1 + \frac{2}{\pi} \arctan\left(1.4 \left(\frac{\Delta}{\delta_s} \right)^2 \right) \right] \tag{8}$$

where α_c is the line loss as calculated using (7) and Δ is the rms surface roughness of the conductor.

Since line loss can be difficult to measure, it is helpful to extract it from the measured quality factor of a resonator, which can be measured accurately. The line loss is related to the quality factor for shorted $\lambda/4$ resonators by [38]

$$Q_{\rm res} = \frac{\beta}{2\alpha_c'} = \frac{\pi}{\alpha_c' \lambda}. \tag{9}$$

C. Frequency Range

A transmission line is typically used at frequencies where only one mode is not cutoff. For TEM transmission lines, the lower cutoff frequency is 0 Hz, or dc. The upper frequency cutoff is set by the next lowest mode that will propagate on the transmission line. Gruner has shown that the mode with the lowest cutoff frequency for a recta-coax line will always be either the TE_{10} or TE_{01} mode [41]. Further, because of symmetry, these modes are the same as the modes in ridged waveguide. The cutoff frequency f_c of the TE_{10} mode in a ridged waveguide occurs when [42]

$$\cot\left(\frac{2\pi t_g f_c}{c} \right) - \left(1 + \frac{w}{2w_g} \right) \tan\left(\frac{t\pi f_c}{c} \right) - \frac{B}{Y_{c1}} = 0 \tag{10}$$

where $c = 2.998 \cdot 10^8$ (m/s) is the speed of light in vacuum and B/Y_{c1} is a shunt susceptance associated with the discontinuity created by the ridge. An approximation for the shunt susceptance can be calculated using [42]

$$\frac{B}{Y_{c1}} = \frac{f_c}{c}(w+2w_g) \left[1 - ln(4u) + \frac{1}{3}u^2 + \frac{1}{2}(1-u^2)^4 \left(\frac{f_c(w+2w_g)}{2c} \right)^2 \right] \tag{11}$$

where $u = 2w_g/(w+2w_g)$. The accuracy of this equation will degrade when $u < 0.5$. However, in this range, the susceptance is not the primary factor in (10) and, thus, the net effect on accuracy is negligible. To find the lowest cutoff frequency, it is necessary to calculate both the TE_{10} and TE_{01} cutoff frequencies. The TE_{01} cutoff frequency can be found using the same equations, but with the widths and thicknesses swapped. A good practice to ensure that operation is well below the cutoff frequency is to include a 15% buffer in the final calculation of the maximum operating frequency $f_{\max}$, resulting in

$$f_{\max} = 0.85 \cdot \min(f_{c,10}, f_{c,01}). \tag{12}$$

III. Fabrication

All of the devices presented in this paper were fabricated through a commercially available three-dimensional (3-D) microfabrication process called EFAB. The authors fabricated devices using a foundry model where design and simulation were done in-house. Design files were then submitted to the vendor, Microfabrica Inc., for fabrication under contract and the devices were returned to the authors for testing. A detailed description of the process is not within the scope of this paper. However, a basic understanding of the process is essential as it impacts the design of the transmission lines. Additional details on EFAB are available in [43] and is also available online.[1]

The EFAB process begins with a planar surface that is suitable for electroplating. On top of this surface, the following three steps are repeated for each desired layer.

Step 1) A patterned sacrificial layer is deposited onto the substrate.

[1][Online]. Available: http://www.microfabrica.com

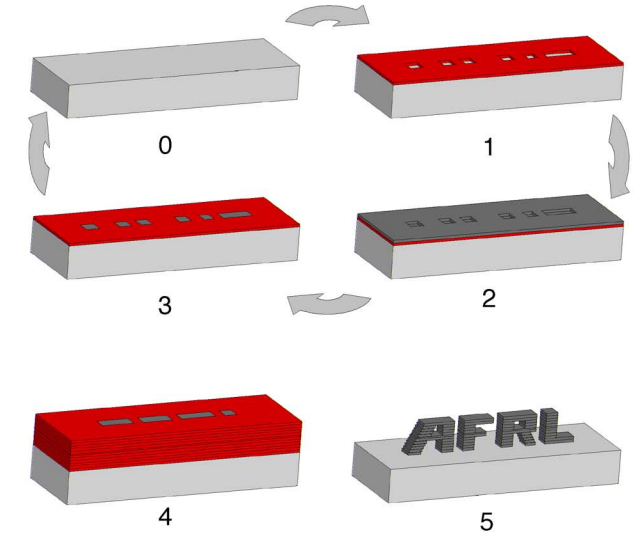

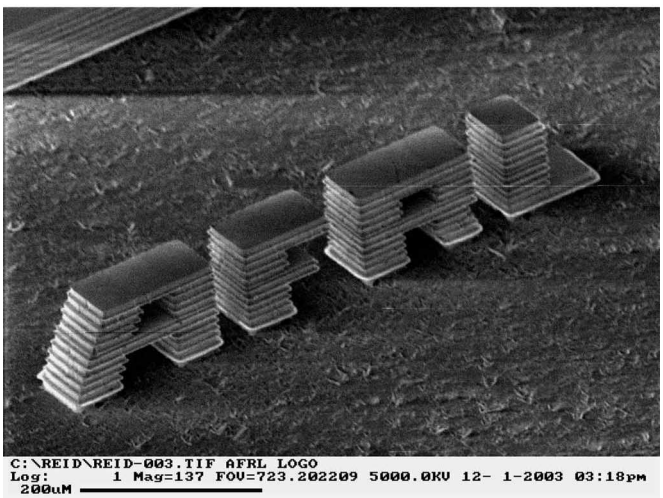

Fig. 2. Schematic illustration of the fabrication of an AFRL logo using the EFAB process. (0) Process begins with planar substrate. (1) Patterned layer is then deposited followed by (2), blanket deposition of a second layer. (3) Top surface is then planarized. Steps (1)–(3) are repeated to create the desired number of layers, as shown in (4). (5) Finally, the sacrificial layer is removed resulting in the desired structure. A scanning electron micrograph (SEM) picture of the realized structure is shown. (Color version available online at: http://ieeexplore.ieee.org.)

Step 2) A second layer, i.e., the structural layer, is blanket deposited over the entire substrate.

Step 3) The top surface is planarized to create a single layer of uniform thickness with two separate materials.

After all of the layers are completed, the sacrificial layer is removed via a chemical etch leaving the structural layers to form the desired structure. A schematic illustration of this process flow is provided in Fig. 2. The process is fundamentally the same as a sacrificial surface micromachining process, with two critical distinctions. First, the layers in this process are typically much thicker ($\approx$ 2–40 μm) than in surface micromachining ($\approx$ 0.5–4 μm). Second, the planarization allows significantly more layers ($\gg$10) than are common in surface micromachining. In the study reported here, three separate fabrication builds were done. The first two builds had 12 layers, while the third had 26 layers. Each run had different layer thicknesses so that the final realized lines had different dimensions. Lines of type A and B from Table I could be realized in build 1, lines of type C could be realized in build 2, and lines of type D and E could be realized in build 3.

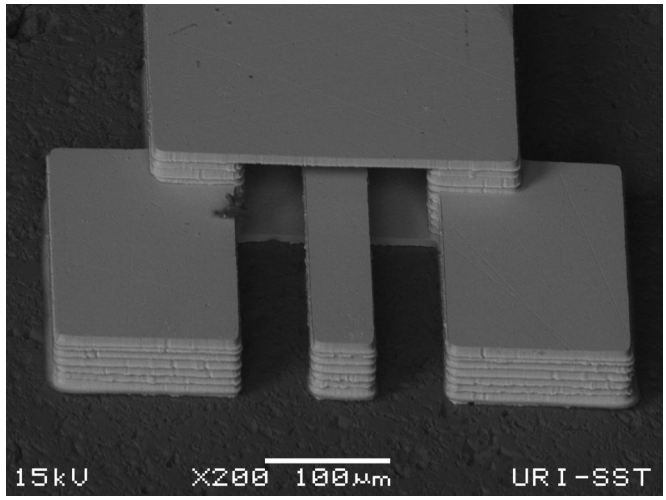

Fig. 3. SEM picture showing the transition from the CPW probe pads to recta-coax line of type A. The line was fabricated with 12 layers of nickel. Scalloping can be seen between each of the layers.

In addition to EFAB, these transmission lines can be fabricated in a number of other processes. Custom processes are available either through in-house development or at several universities [16]–[20], [44]–[46]. In addition, the Defense Advanced Research Projects Agency (DARPA) 3-D microelectromagnetic RF systems (MERFS) program aims to develop a low-cost multilayer process utilizing copper as the structural material. This process uses layers that are even thicker than the EFAB layers to minimize the number of masking steps and, thus, reduce the costs for recta-coax lines.[2]

IV. Results

A. Impedance

Designing recta-coax lines using a layered sacrificial process such as EFAB requires certain considerations. The layered nature of these processes can result in scalloping at the layer interfaces, as is visible in Fig. 3. In order to mitigate any effects this might have on the impedance of the lines, all of our lines are designed so the ratio of linewidth to gap thickness is always greater than the ratio of thickness to gapwidth or $(w/t_g) > (t/w_g)$. Thus, the capacitance from the signal line is always dominated by the capacitances associated with the top and bottom ground planes and the capacitance to the sidewalls is reduced. In addition to the scalloping, there is some concern with layer-to-layer misalignment. To date, neither of these concerns has had a measurable effect on our devices. In addition to these concerns, sacrificial etching requires the regular, but not necessarily periodic, spacing of etch access holes. These holes are visible in Fig. 4. However, the design constraint mentioned above also mitigates this problem. Preliminary electromagnetic simulations indicate

[2][Online]. Available: http://www.darpa.mil/MTO/people/pms/evans/3dmerfs.html

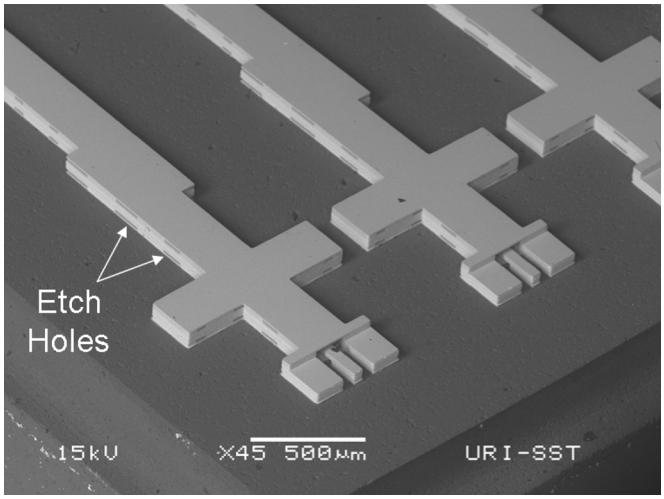

Fig. 4. SEM picture showing the ports for two 60-GHz bandpass filters. Etch access holes are visible on the sidewalls of the filters.

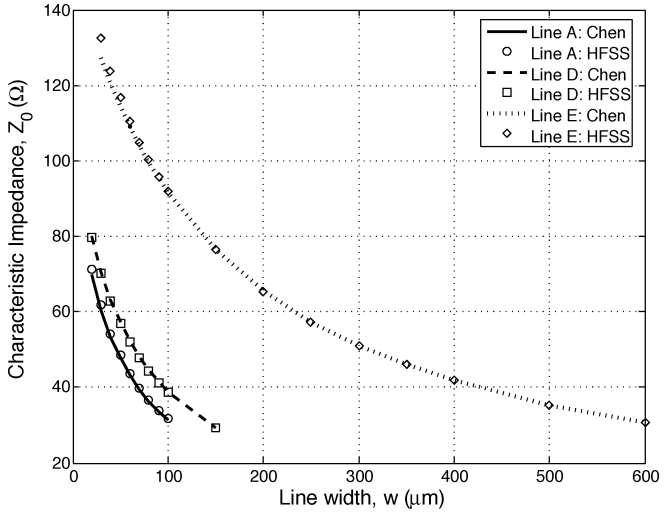

Fig. 5. Impedance of three different lines plotted as a function of linewidth. The continuous lines are modeled values, while the discrete points are simulated values.

that etch holes have only a negligible effect when the transmission lines are used for signal routing and nonresonant devices. However, in resonator designs, the etch holes may play a more significant role, and further investigations are required.

Recta-coax lines are designed by first selecting t, and t_g based on selected layer thicknesses. Next, w_g is fixed so that the sidewall capacitance is lower than the top and bottom wall capacitances. Based on this, calculations of the characteristic impedance were compared to HFSS simulations for lines of type A, D, and E in Table I. These geometries were specifically chosen to cover a wide range of possible aspect ratios. The results of these calculations are shown in Fig. 5. The calculations based on (1)–(3) agree well with the simulated port impedances with the only significant (>2%) variations occurring for line type E at high impedances over 115 Ω. This is not surprising, as these lines violate the $w > w_g$ accuracy criteria for the capacitance model. The width required to achieve a 50-Ω line for types A–E is reported in Table II in the w_{50} column. As can be seen, lines of type B are not realistic due to the very narrow width required to achieve 50 Ω. Lines of the other four types have been realized in three separate fabrication runs.

Fig. 6 shows a comparison of the measured and simulated characteristic impedance Z_0 of recta-coax lines. The impedance was calculated from both the measured and simulated S-parameters using the conventional single-line technique described in [47]. The cross-sectional dimensions of the line are those of Line A in Table I, with the center conductor width at 47 μm, corresponding to a simulated port impedance of 50 Ω. The measured lines are nominally identical with a length of 1.1 mm. The vector network analyzer was calibrated to a reference impedance of 50 Ω at the probe tips using the short, open, load, thru (SOLT) method with the probe manufacturers calibration substrate. The measured S-parameters include effects of the coplanar-to-recta-coax transition, while the electromagnetic simulation does not include transitions. The mean value of the measured Z_0 over the measured frequency range is $48.11 - j0.04\ \Omega$. This compares well with the mean value of the simulated Z_0 at $48.05. - j0.82\ \Omega$.

TABLE II
50 Ω LINEWIDTHS AND MAXIMUM OPERATING FREQUENCIES FOR DIFFERENT RECTA-COAX LINES

Line	w_{50} (μm)	f_{max} (GHz)
A	47	741.3
B	7	1,591.1
C	60	579.2
D	65	672.5
E	309	201.6

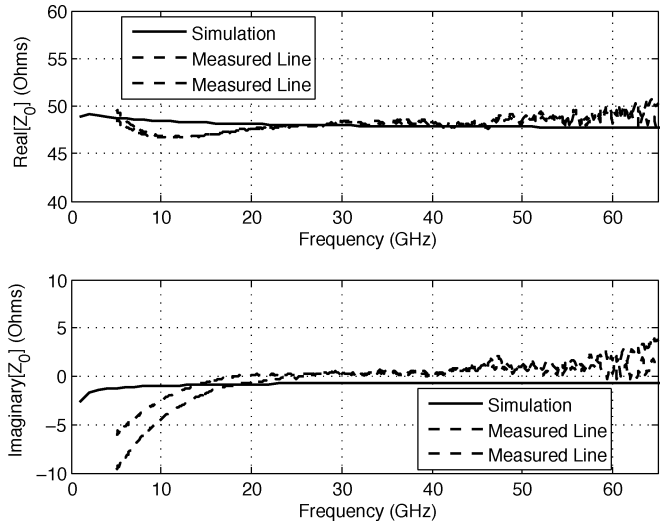

Fig. 6. Characteristic impedance Z_0 of measured recta-coax lines is compared to Z_0 of an electromagnetic simulation of the lines. The line dimensions are those of Line A in Table I, with a center conductor width of 47 μm, corresponding to a simulated port impedance of 50 Ω. The measured lines are nominally identical with a length of 1.1 mm. Coplanar to recta-coax transitions are included in the measurements.

B. Line Loss

The loss for lines A, D, and E was calculated using (7) and (8). The loss for these lines fabricated in nickel ($\sigma = 1.45 \cdot 10^5$ s/m) is presented in Fig. 7 in terms decibels/centimeter. For all of the loss calculations, a surface roughness of $\Delta = 0.065$ μm is used. This value was measured from the top surface of the build

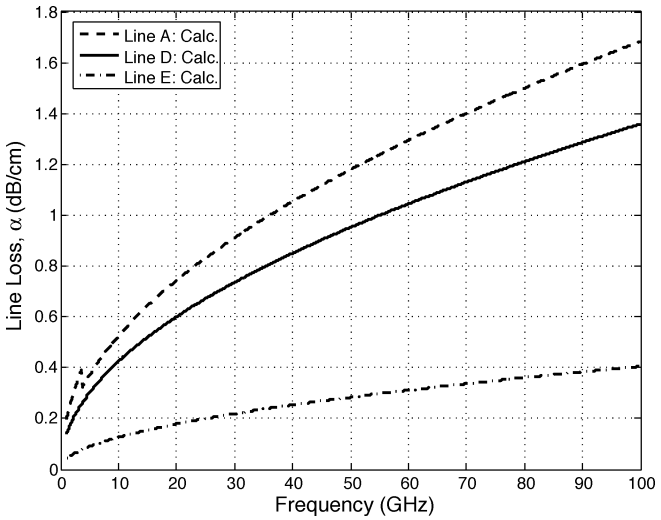

Fig. 7. Modeled line loss for 50-Ω nickel lines of types A, D, and E.

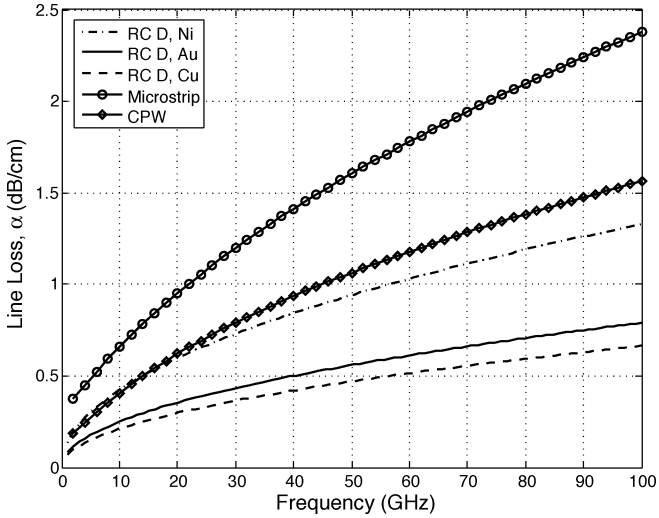

Fig. 8. Comparison of the modeled line loss for recta-coax line type D with 50-Ω microstrip line on a 50-μm-thick GaAs substrate, and a 50-Ω CPW on a sapphire substrate with a linewidth of 80 μm and a gap of 40 μm. Both the microstrip and CPW lines are simulated using 2-μm-thick gold.

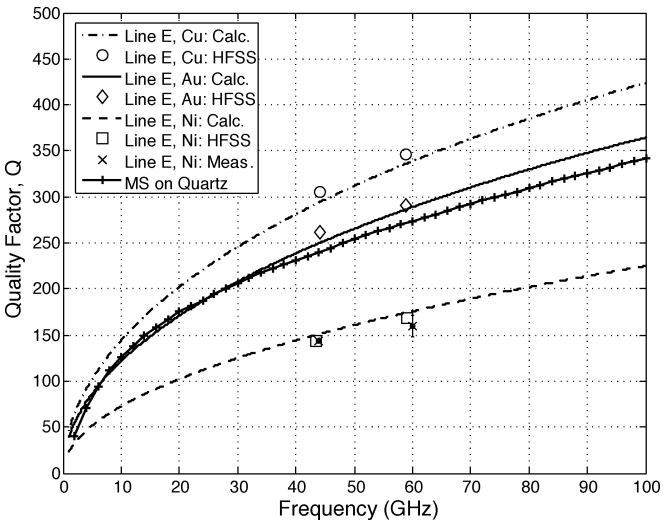

Fig. 9. Measured quality factor of nickel $\lambda/4$ resonators compared with modeled quality factors for lines of different metallizations and a 50-Ω microstrip line on 150-μm-thick fused silica with a 2-μm-thick gold metallization.

1 recta-coax signal lines using a optical profilometer. Based on (8), this increases the loss of the nickel lines by less than 3% over the entire frequency range. At the time of fabrication, nickel was the only metal available through EFAB. Metals such as gold, copper, and silver offer significantly lower losses, and Fig. 8 provides a comparison between line type D in nickel, gold, and copper to circuit simulations of 50-Ω microstrip on 50-μm-thick GaAs and 50-Ω CPW on sapphire. The microstrip line has a width of 35 μm and is simulated with a 2-μm-thick gold metallization. This line was chosen because 50-μm GaAs is an industry standard. The CPW line dimensions are those used in the design of microwave microelectromechanical systems (MEMS) switches at the Air Force Research Laboratory (AFRL), Hanscom AFB, MA [48], [49]. These lines are also simulated with a 2-μm-thick gold metallization. Recta-coax line type D was chosen because it yields lines that are generally comparable in size. A 50-Ω line of type D has a total width of 195 μm including the line, gaps, and ground walls. This is significantly more than the 35-μm-wide microstip. However, the microstrip line generally needs a buffer of at least 1.5–2 linewidths on each side, resulting in a total path width that is 140–175 μm. As shown in the comparison, recta coax is relatively low loss in terms of decibels/centimeter even when it is fabricated with nickel.

While the loss per unit length is important for signal routing across a die, many circuits are more concerned with loss as a function of electrical length. In this case, loss per wavelength $(\alpha\lambda)$ or resonator quality factor $(Q_{\rm res})$ are more appropriate measures of line performance. From (9), it is clear that quality factor is inversely proportional to the loss per wavelength. Since resonator quality factor can be measured accurately, independent of the calibration, quality factor is presented here. The quality factor of $\lambda/4$ shorted resonators is presented in Fig. 9 for line type E with nickel, gold, and copper metallizations. For comparison, the calculated loss of 50-Ω microstrip lines on a 15-μm-thick fused silica substrate are also provided. On 150-μm-thick silica, the microstrip lines are calculated to be 324-μm wide. The microstrip line loss is calculated using Agilent ADS with a 2-μm-thick gold line. Recta-coax resonators fabricated with nickel have lower quality factors than the microstrip lines. However, when gold or copper are used, the recta-coax compares well with the microstrip line. The final choice of a metal must also consider the mechanical properties of the material and environmental factors such as corrosion. While nickel has relatively low conductivity, it has a relatively high Young's modulus, leading to mechanical strength and rigidity. This allows nickel lines to be suspended for several millimeters without significant deviation from the design parameters. We are currently investigating plating the nickel lines with gold to provide a mechanically strong line with low electrical loss. At millimeter-wave frequencies, a nickel line plated with 1–2 μm of gold would provide good mechanical strength, low electrical loss, and a corrosion resistant surface. The loss calculations are verified by measuring the quality factors of $\lambda/4$, line type E, shorted resonators at 44 and 60 GHz. Measurements were taken

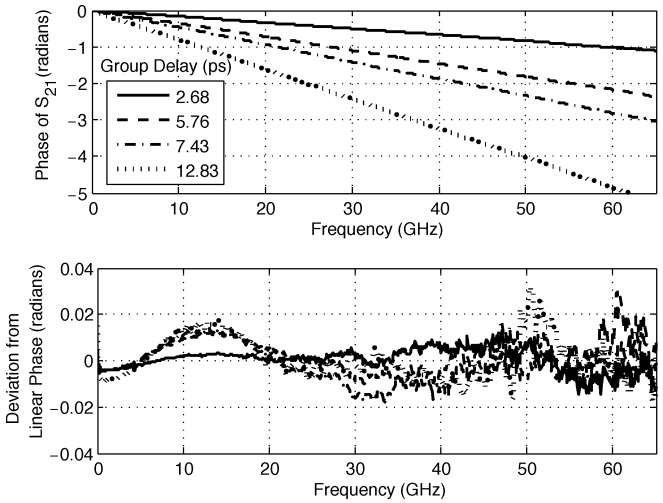

Fig. 10. Measured phase of S_{21} versus frequency for four recta-coax lines and the deviation from linear phase indicate low dispersion. The line dimensions are those of line A in Table I, with a center conductor width of 47 μm, corresponding to a simulated port impedance of 50 Ω. The line lengths are 0.2, 1.1, 1.6, and 3.2 mm. Coplanar to recta-coax transitions are included in the measurements.

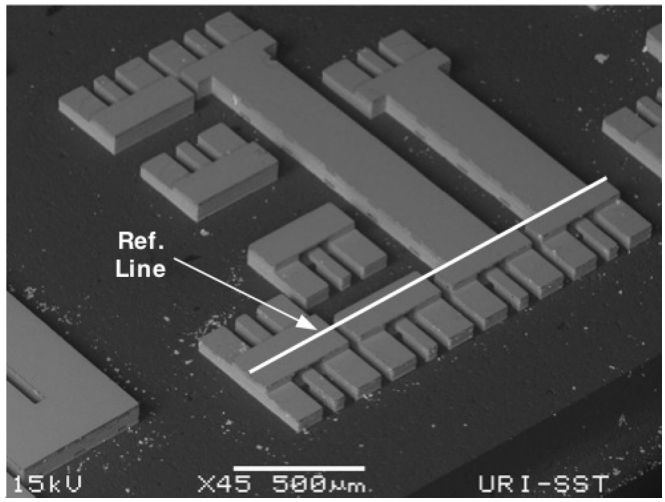

Fig. 11. TRL calibration set. The thru is the short line in the lower left. The lines are 1.1- and 1.6-mm long. The four reflect standards are implemented to facilitate easy probing.

on nine 44-GHz resonators, and ten 60-GHz resonators located on five different die. The average measured quality factors were 142.8 and 155.8 at 44 and 60 GHz, respectively. These values are slightly below the HFSS simulations (145 and 169, respectively) and the calculated values (150.9 and 175.7, respectively), but are generally in good agreement. This corresponds to a line loss of 0.282 dB/cm at 44 GHz and 0.353 dB/cm at 60 GHz.

C. Dispersion and Group Velocity

The measured transmission phase for four 50-Ω lines shown in Fig. 10. The line lengths are 0.2, 1.1, 1.6, and 3.2 mm and the corresponding group delays obtained from a linear fit to the phase curves are 2.68, 5.76, 7.43, and 12.83 ps. These measurements were taken using a SOLT calibration and, therefore, do include coplanar-to-recta-coax transitions. The deviation from linear phase remains within $+/-0.02$ rad, except for a few spikes above 50 GHz. A linear regression of the delays on the line lengths gives a group velocity of $2.958 \cdot 10^8$ m/s. This value is within 1.5% of the speed of light expected for an air dielectric recta-coax line.

D. Operation Frequency

The operational frequency ranges for 50-Ω recta-coax lines of types A–E calculated using (10)–(12) are presented in Table II. It can be seen that for types A–D, the maximum operating frequencies are well in excess of 500 GHz, while for type E, it is over 200 GHz.

E. Thru-Reflect-Line (TRL) Calibration Standard

In order to facilitate measurements, a TRL calibration set is implemented on chip with each die. The TRL from our first build was implemented using 50-Ω lines of type A. This cal set is shown in Fig. 11. Measurements are taken using ground–signal–ground probes with a 0.15-mm center-to-center spacing. Since the coax can not be directly probed, it was necessary to terminate the lines in a thick CPW section that is designed to have a 50-Ω characteristic impedance. This CPW section extends 0.2 mm from the beginning of the recta-coax. It is designed so that the center conductor does not have to change height or width, but there is a transition in the ground at the entrance to the recta-coax.

The TRL set includes a 0.2-mm thru, multiple reflect standards that have 0.1 mm of line length, 1.1- and 1.6-mm lines. As a result, the TRL calibration sets the measurement reference plane 0.1 mm in from the entrance to the recta-coax. Using the TRL set will then exclude any effects caused by the transitions from probe to CPW to recta coax. The accuracy of the TRL calibration is generally best when the electrical length of the lines is 30°–150° Therefore, this TRL set is good from 16.7 to 125 GHz. Typically, when the TRL calibration set is used, measurements are taken from 30 to 67 GHz.

F. Line With Bends

One of the reported advantages of these lines is their ability to turn corners without significant design issues. As such, a demonstration line was fabricated with four 90° bends. This line is shown in Fig. 12. The total length of the bent line is 3.2 mm measured on a path running along the center of the line with cross-sectional dimensions of line type A. Fig. 13 shows the measured scattering parameters for the 3.2-mm line with four bends compared to a 3.2-mm straight line. The two lines appear almost identical with the average loss always within 0.3 dB. Measurements from multiple lines typically show the bent lines to have 5°–10° less phase shift at 60 GHz. However, an accurate characterization of the bend will require implementing it in a resonator type structure. As is clear in Fig. 12, the line is routed in an S-configuration with all three sections close to each other. The ground lines are spaced 54 μm apart for a center to center spacing of 302 μm. This is only possible because of the signal isolation achieved by having and enclosed TEM line, and this feature of the transmission lines can be used to make devices like branch-line couplers significantly more compact, as demonstrated by Chen *et al.* [21].

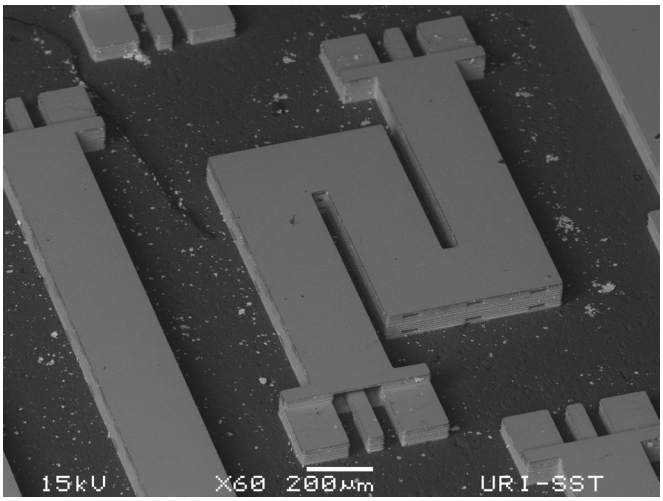

Fig. 12. 3.2-mm line (50-Ω type A) with four 90° bends.

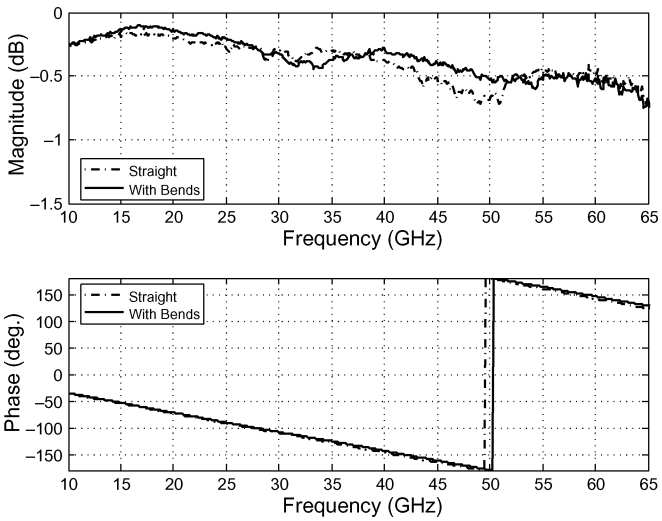

Fig. 13. Measured scattering parameters for two 3.2-mm-long lines. One of the lines is straight while the other has four 90° bends.

G. 60-GHz Branch-Line Coupler

In order to demonstrate the performance of these transmission lines, a branch-line coupler was realized at 60 GHz [23]. The coupler can be seen in Fig. 14, and Table III provides the widths and characteristic impedances for the two arms. Over a 10% bandwidth (57–63 GHz), the two coupled lines have measured average insertion loss of −3.625 and −3.870 dB. The measured insertion loss of these paths is within 0.25 dB of the design simulation, while the measured phase is within 5° of the original simulation. In order to save space on the die, a second test structure was inserted inside the coupler. The inserted test structure places metal walls 50 μm from the cross arms of the branch-line coupler. This structure, visible in Fig. 14, is an unrelated test structure and was not included in any of the coupler simulations.

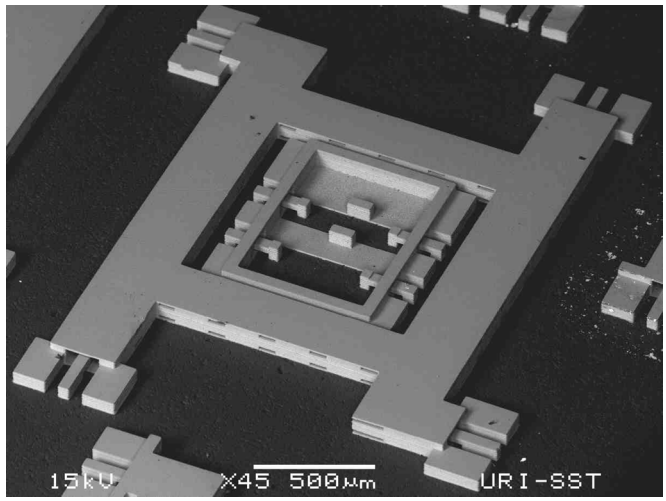

Fig. 14. SEM picture showing a 60-GHz branch-line coupler.

TABLE III
LINE DIMENSIONS FOR A 60-GHz BRANCH-LINE COUPLER USING LINE TYPE A

Line	t	w	t_g	w_g	Length	$Z_0(\Omega)$
L1	0.028	0.024	0.086	0.05	1.26	35.6
L2	0.028	0.024	0.046	0.05	1.26	51.4

(All dimensions in mm)

H. Cross Overs

In the third build, a six-port coupler was implemented. This coupler is shown in Fig. 15. Detailed design and testing of this coupler are provided in [25]; however, the coupler is shown here because the physical implementation requires lines that cross over. These cross overs are shown in Fig. 15. Simulations of the coupler showed no significant crosstalk between the two line layers. As with the branch-line coupler, the measured coupler performs exactly as designed.

V. DISCUSSION

Design equations for recta-coax lines have been presented for impedance, loss, and frequency range. Calculations of impedance, loss, and resonator quality factor are shown to be in good agreement with full-wave electromagnetic simulations over a range of design parameters. Measured line impedance is shown to agree very well with simulated line impedance over a wide frequency range. Measured lines showed losses consistent with the calculated values. However, for better accuracy, resonators were measured at two frequencies and are shown to be in good agreement with predictions. In addition, the group velocity of the lines was measured and the line dispersion was shown to be very low up to 67 GHz.

Integrated recta-coax lines offer significant advantages over microstrip and CPW lines for millimeter-wave circuit design. We have presented many of these advantages here and in previous work including low-loss 180° bends, signal cross overs, and isolation of signals. Recta-coax lines have also been shown

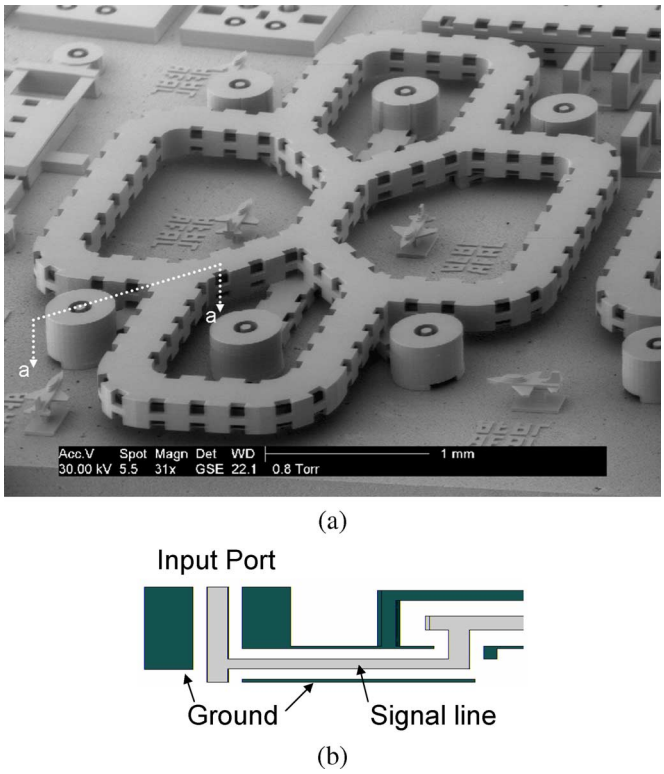

Fig. 15. (a) SEM picture of a six-port coupler. The six circular structures are probe ports used for testing. The couplers ports are located at the junctions. The probe ports are connected the coupler ports by transmission lines running under the coupler and then rising up to the coupler signal lines, as illustrated in the a–a cutaway shown in (b). (Color version available online at: http://ieeexplore.ieee.org.)

to have relatively low losses compared to both microstrip and CPW lines. This is true when considering loss over a given distance (decibels/centimeters), loss per wavelength, or resonator quality factor. Due to the air dielectric, recta-coax resonators are physically longer than either microstrip or CPW resonators at the same frequency, but even when the recta-coax lines are fabricated with nickel, the resulting quality factor is comparable. The eventual use of either plated lines or copper lines will dramatically improve the quality factor of recta-coax resonators. The ability to repeatably realize resonators with quality factors above 100 will make this technology suitable to applications including filters and oscillators.

Recta-coax lines do require a more complicated fabrication process than either CPW or microstrip lines. At this time, it is not possible to do an accurate cost comparison between the technologies because the recta-coax processes are still relatively immature. However, as this technology develops, this comparison will need to take into account the reduced design cost that should be possible with recta-coax lines. Reduced design costs are anticipated because recta-coax lines can be designed independent of the substrate and independent of the surrounding environment. As an example, we have presented a branch-line coupler and noted that, after the design was completed, a structure was added to the center area of the coupler with no effect on simulated performance. In fact, at this point, all of the designs we have completed have been done independently, and then placed on the substrate considering only the need to physically probe the devices. This greatly simplifies the design issues involved in millimeter-wave circuits, and can possibly lead to a much higher level of integration.

ACKNOWLEDGMENT

This paper has been cleared for public release: Distribution Unlimited (ESC06-0062).

REFERENCES

[1] N. Dib, W. Harokopus, L. Katehi, C. Ling, and G. Rebeiz, "Study of a novel planar transmission line," in *IEEE MTT-S Int. Microw. Symp. Dig.*, Jun. 1991, pp. 623–626.

[2] N. Dib and L. Katehi, "Impedance calculation for the microshield line," *IEEE Trans. Microw. Guided Wave Lett.*, vol. 2, no. 10, pp. 406–408, Oct. 1992.

[3] L. Katehi, G. Rebeiz, T. Weller, R. Drayton, H.-J. Cheng, and J. Whitaker, "Micromachined circuits for millimeter- and sub-millimeter-wave applications," *IEEE Antennas Propag. Mag.*, vol. 35, no. 5, pp. 9–17, Oct. 1993.

[4] T. Weller, L. Katehi, and G. Rebeiz, "High performance microshield line components," *IEEE Trans. Microw. Theory Tech.*, vol. 43, no. 3, pp. 534–543, Mar. 1995.

[5] C.-Y. Chi and G. Rebeiz, "Conductor-loss limited stripline resonators and filters," *IEEE Trans. Microw. Theory Tech.*, vol. 44, no. 4, pp. 626–630, Apr. 1996.

[6] S. Robertson, L. Katehi, and G. Rebeiz, "Micromachined W-band filters," *IEEE Trans. Microw. Theory Tech.*, vol. 44, no. 4, pp. 598–606, Apr. 1996.

[7] P. Blondy, A. Brown, D. Cros, and G. Rebeiz, "Low-loss micromachined filters for millimeter-wave communication systems," *IEEE Trans. Microw. Theory Tech.*, vol. 46, no. 12, pp. 2283–2288, Dec. 1998.

[8] A. Brown and G. Rebeiz, "A high-performance integrated K-band diplexer," *IEEE Trans. Microw. Theory Tech.*, vol. 47, no. 8, pp. 1477–1481, Aug. 1999.

[9] A. Margomenos, K. Herrick, M. Herman, S. Valas, and L. Katehi, "Isolation in three-dimensional integrated circuits," *IEEE Trans. Microw. Theory Tech.*, vol. 51, no. 1, pp. 25–32, Jan. 2003.

[10] V. Milanović, M. Gaitan, E. Bowen, and M. Zaghloul, "Micromachined coplanar waveguides in CMOS technology," *IEEE Trans. Microw. Guided Wave Lett.*, vol. 6, no. 10, pp. 380–382, Oct. 1996.

[11] ——, "Micromachined microwave transmission lines in CMOS technology," *IEEE Trans. Microw. Theory Tech.*, vol. 45, no. 5, pp. 630–635, May 1997.

[12] J. R. Thorpe, D. P. Steenson, and R. E. Miles, "High frequency transmission line using micromachined polymer dielectric," *Electron. Lett.*, vol. 34, no. 12, pp. 1237–1238, Jun. 1998.

[13] D. Newlin, A.-V. H. Pham, and J. Harriss, "Development of low loss organic-micromachined interconnects on silicon at microwave frequencies," *IEEE Trans. Compon. Packag. Technol.*, vol. 25, no. 3, pp. 506–510, Sep. 2002.

[14] W. Y. Liu, D. P. Steenson, and M. B. Steer, "Membrane-supported CPW with mounted active devices," *IEEE Microw. Wireless Compon. Lett.*, vol. 11, no. 4, pp. 167–169, Apr. 2001.

[15] F. D. Mbairi and H. Hesselbom, "High frequency design and characterization of SU-8 based conductor backed coplanar waveguide transmission lines," in *Proc. Int. Adv. Packag.: Processes, Properties, Interfaces Symp.*, Mar. 2005, pp. 243–248.

[16] J.-B. Yoon, B.-I. Kim, Y.-S. Choi, and E. Yoon, "3-D lithography and metal surface micromachining for RF and microwave MEMS," in *IEEE Int. Microelectromech. Syst. Conf.*, Jan. 2002, pp. 20–24.

[17] E.-C. Park, Y.-S. Choi, B.-I. Kim, J.-B. Yoon, and E. Yoon, "A low loss MEMS transmission line with shielded ground," in *IEEE Int. Microelectromech. Syst. Conf.*, Jan. 2003, pp. 136–139.

[18] J.-B. Yoon, B.-I. Kim, Y.-S. Choi, and E. Yoon, "3-D construction of monolithic passive components for RF and microwave ICs using thick-metal surface micromachining technology," *IEEE Trans. Microw. Theory Tech.*, vol. 51, no. 1, pp. 279–288, Jan. 2003.

[19] E.-C. Park, T.-S. Song, S.-H. Baek, and E. Yoon, "Low phase noise CMOS distributed oscillators using MEMS low loss transmission lines," in *IEEE Int. Microelectromech. Syst. Conf.*, Jan. 2004, pp. 645–648.

[20] H.-S. Lee, D.-H. Shin, S.-C. Kim, B.-O. Lim, T.-J. Baek, B.-S. Ko, Y.-H. Chun, S.-K. Kim, H.-C. Park, and J.-K. Rhee, "Fabrication of new micromachined transmission line with dielectric posts for millimeter-wave applications," *J. Micromech. Microeng.*, vol. 14, pp. 746–749, 2004.
[21] R. Chen, E. Brown, and C. Bang, "A compact low-loss Ka-band filter using 3-dimensional micromachined integrated coax," in *IEEE Int. Microelectromech. Syst. Conf.*, Jan. 2004, pp. 801–804.
[22] E. Brown, A. Cohen, C. Bang, M. Lockard, G. Byrne, N. Vendelli, D. McPherson, and G. Zhang, "Characteristics of microfabricated rectangular coax in the Ka band," *Microw. Opt. Technol. Lett.*, vol. 40, pp. 365–804, Mar. 2004.
[23] J. Reid and R. Webster, "A 60 GHz branch line coupler fabricated using integrated rectangular coaxial lines," in *IEEE MTT-S Int. Microw. Symp. Dig.*, Jun. 2004, pp. 441–444.
[24] ——, "A compact integrated coaxial V-band bandpass filter," in *IEEE AP-S Int. Symp. Dig.*, Jun. 2004, pp. 990–993.
[25] ——, "A six-port 60 GHz coupler for an rn^2 beam former," in *IEEE AP-S Int. Symp. Dig.*, Jul. 2006.
[26] ——, "A 55 GHz bandpass filter realized with integrated TEM transmission lines," in *IEEE MTT-S Int. Microw. Symp. Dig.*, Jun. 2006, pp. 132–135.
[27] High Frequency Structure Simulator (HFSS) ver. 9.0, Ansoft Corporation, Palo Alto, CA [Online]. Available: http://www.ansoft.com
[28] T.-S. Chen, "Determination of the capacitance, inductance and characteristic impedance of rectangular lines," *IRE Trans. Microw. Theory Tech.*, vol. MTT-8, no. 9, pp. 510–519, Sep. 1960.
[29] C. Weil, "The characteristic impedance of rectangular transmission lines with thin center conductor and air dielectric," *IEEE Trans. Microw. Theory Tech.*, vol. MTT-26, no. 4, pp. 238–242, Apr. 1978.
[30] S. Cohn, "Thickness corrections for capacitive obstacles and strip conductors," *IRE Trans. Microw. Theory Tech.*, vol. MTT-9, no. 11, pp. 638–644, Nov. 1961.
[31] W. Getsinger, "Coupled rectangular bars between parallel plates," *IRE Trans. Microw. Theory Tech.*, vol. MTT-10, no. 9, pp. 65–72, Sep. 1962.
[32] R. Garver, "Z_0 of rectangular coax," *IRE Trans. Microw. Theory Tech.*, vol. MTT-9, no. 5, pp. 262–263, May 1961.
[33] O. Cruzan and R. Garver, "Characteristic impedance of rectangular coaxial transmission lines," *IRE Trans. Microw. Theory Tech.*, vol. MTT-12, no. 9, pp. 488–495, Sep. 1964.
[34] H. Riblet, "The exact dimensions of a family of rectangular coaxial lines with given impedance," *IEEE Trans. Microw. Theory Tech.*, vol. MTT-20, no. 8, pp. 538–541, Aug. 1972.
[35] ——, "An approximation for the characteristic impedance of shielded-slab line," *IEEE Trans. Microw. Theory Tech.*, vol. MTT-27, no. 6, pp. 557–559, Aug. 1979.
[36] ——, "Two limiting values of the capacitance of symmetrical rectangular coaxial strip transmission line," *IEEE Trans. Microw. Theory Tech.*, vol. MTT-29, no. 7, pp. 661–666, Aug. 1981.
[37] J. Tippet and D. Chang, "Characteristic impedance of a rectangular coaxial line with offset inner conductor," *IEEE Trans. Microw. Theory Tech.*, vol. MTT-26, no. 11, pp. 876–883, Nov. 1978.
[38] D. Pozar, *Microwave Engineering*. Reading, MA: Addison-Wesley, 1990.
[39] K. Lau, "Loss calculations for rectangular coaxial lines," *Proc. Inst. Elect. Eng.*, vol. 135, no. 3, pp. 207–209, Jun. 1988.
[40] T. Edwards, *Foundations for Microstrip Circuit Design*, 2nd ed. New York: Wiley, 1992.
[41] L. Gruner, "Higher order modes in rectangular coaxial waveguides," *IEEE Trans. Microw. Theory Tech.*, vol. MTT-15, no. 8, pp. 483–485, Aug. 1967.
[42] R. Collin, *Foundations for Microwave Engineering*, 2nd ed. New York: McGraw-Hill, 1992.
[43] A. Cohen, G. Zhang, F. Tseng, F. Mansfield, U. Frodis, and P. Will, "EFAB: Rapid low-cost desktop micromachining of high aspect ratio true 3-D MEMS," in *IEEE Int. Microelectromech. Syst. Conf.*, Jan. 1999, pp. 244–251.
[44] Y.-J. Kim and M. Allen, "Surface micromachined solenoid inductors for high frequency applications," *IEEE Trans. Compon., Packag., Manuf. Technol.*, vol. 21, no. 1, pp. 26–33, Jan. 1998.
[45] Y.-H. Joung, S. Nuttinck, S.-W. Yoon, M. Allen, and J. Laskar, "Integrated inductors in the chip-to-board interconnect layer fabricated using solderless electroplating bonding," in *IEEE MTT-S Int. Microw. Symp. Dig.*, Jun. 2002, pp. 1409–1412.
[46] S. Pinel, F. Cros, S. Nuttinck, S.-W. Yoon, M. Allen, and J. Laskar, "Very high-Q inductors using RF-MEMS technology for system-on-package wireless communication integration module," in *IEEE MTT-S Int. Microw. Symp. Dig.*, Jun. 2003, pp. 1497–1500.
[47] W. Eisenstadt and Y. Eo, "S-parameter-based IC interconnect transmission line characterization," *IEEE Trans. Compon., Hybrids, Manuf. Technol.*, vol. 15, no. 4, pp. 483–490, Aug. 1992.
[48] J. Reid, L. Starman, and R. Webster, "RF actuation of capacitive MEMS switches," in *IEEE MTT-S Int. Microw. Symp. Dig.*, Jun. 2003, pp. 1919–1922.
[49] J. Ebel, R. Corez, K. Leedy, and R. Strawser, "Hermetic thin-film encapsulation for RF MEMS switches," in *Proc. Gomactech*, 2005, pp. 327–330.

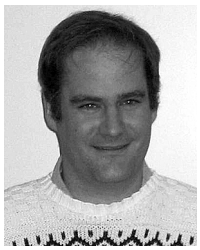

J. Robert Reid (S'94–M'97) received the B.S.E.E. degree from Duke University, Durham, NC, in 1992, and the M.S.E.E. and Ph.D. degrees from the Air Force Institute of Technology (AFIT), Dayton, OH, in 1993 and 1996, respectively.

He is currently an Electronics Engineer with the Antenna Technology Branch, Electromagnetics Technology Division, Air Force Research Laboratory (AFRL), Hanscom AFB, MA. In 1992, he was commissioned a second lieutenant with the US Air Force and sent to the AFIT. Since 1997, he has been with the AFRL, where he conducts research into the application of micromachining and MEMS to front-end antenna technology. In 2002, he separated from the Air Force and joined the AFRL as a civilian. His current research includes design, fabrication, and testing of micromachined transmission lines, RF MEMS switches and varactors, millimeter-wave phase shifters, and switching networks.

Dr. Reid is a member of Sigma Xi.

Eric D. Marsh (S'03–M'04) received the Bachelor's degree in electrical engineering from Iowa State University, Ames, in 1999, and the Master's degree in electrical engineering from the Air Force Institute of Technology, Dayton, OH, in 2004.

In 1999, he joined the United States Air Force as a Developmental Engineer. Since 2004, he has been with the Sensor's Directorate, Air Force Research Laboratory, Hanscom AFB, MA, where he performs basic research on micromachined millimeter-wave transmission lines and components.

Richard T. Webster (S'76–M'76–SM'02) received the B.S. and M.E. degree in electrical engineering from the Rensselaer Polytechnic Institute, Troy, NY, in 1973 and 1976, respectively.

He is currently an Electronics Engineer with the Antenna Technology Branch, Electromagnetics Technology Division, Air Force Research Laboratory (AFRL), Hanscom AFB, MA. Since 1980, he has been with the AFRL, where he plans and conducts programs to develop monolithic microwave and millimeter-wave integrated circuits for amplification and signal control in phased-array antenna systems. His current research is focused on the development of amplifiers, switches, phase shifters, and related components using a variety of technologies including semiconductor, microelectromechanical, and electromagnetic.

Mr. Webster is a member of Sigma Xi.